Surface Preparation and In/Ga Alloying Effects on InGaAs(001)-(2x4) Surfaces For ALD Gate Oxide Deposition

Mary Edmonds[a, b], Wilhelm Melitz[a, b], Tyler J. Kent[a, b], Evgueni Chagarov[a], and Andrew C. Kummel[a]

[a]Department of Chemistry and Biochemistry, [b]Materials Science & Engineering Program
University of California, San Diego, La Jolla, CA 92093, USA

High resolution STM images of $In_{0.53}Ga_{0.47}As(001)$-(2x4) were obtained and surface defects were quantified as a function of sample preparation technique. Published STM images of InGaAs(001)–(2x4) samples of varying In composition were examined and missing dimer unit cells, adatom trough defects, and incomplete atomic terraces were quantified for comparison with the $In_{0.53}Ga_{0.47}As(001)$-(2x4) surface. Density Functional Theory (DFT) modeling of α2(2x4) and β2(2x4) unit cell constructions and electronic structures show that the missing dimer defect creates conduction band edge states not readily passivated by trimethy aluminum; therefore, the density of dimer defects may cause trap state formation at oxide/InGaAs(001) interfaces.

Introduction

As silicon based metal oxide semiconductor field effect transistors (MOSFETs) approach their performance limits, alternative materials are being explored for use in the channel region. $In_{0.53}Ga_{0.47}As$ has an intrinsically high electron mobility making it an attractive alternative semiconductor material for use in MOSFET applications (1). Scanning tunneling spectroscopy (STS) has been employed to show that the As-rich (2x4) surface reconstruction of $In_{0.53}Ga_{0.47}As(001)$ contains an electrically unpinned surface Fermi level both pre and post trimethylaluminum (TMA) dosing (2). The unpinned electronic structure along with the highly ordered dense adsorbate structure of $TMA/In_{0.53}Ga_{0.47}As(001)$-(2x4) makes it an appealing candidate for nucleation of gate oxide on $In_{0.53}Ga_{0.47}As(001)$ (2,3). The scaling of gate oxides requires ALD precursor nucleation in every unit cell of the semiconductor channel surface (4). The semiconductor oxide interface greatly impacts device performance via either interfacial roughness or formation of defects containing electronic trap states that hinder Fermi level modulation by the gate potential (2). Therefore, reduction of defects and contaminants on the initial III-V surface is necessary to minimize the D_{it} (2).

Density functional theory (DFT) is used to model the atomic configurations and electrical properties of ideal and missing dimer unit cells on the InGaAs(001)-(2x4) surface. The simulations show that the missing As dimer defect sites have conduction band edge states which the ideal double As dimer unit cells lack and which cannot be passivated by TMA chemisorption. The defect densities observed on the $In_{0.53}Ga_{0.47}As(001)$-(2x4) surface are compared to defect densities on similar As-rich reconstructions of GaAs(001)-(2x4), low and high In content InGaAs(001)-(2x4), and

InAs(001)-(2x4) to determine the relative roles of strain and surface bond strengths on defect formation. The effectiveness of an atomic hydrogen cleaning technique to remove the native oxide and restore the $In_{0.53}Ga_{0.47}As$(001)-(2x4) surface to the order and cleanliness of MBE grown samples are reported. Surface defects on samples before and after hydrogen dosing as well as after a post cleaning anneal process are quantified to determine to role of the surface preparation technique upon defect density.

Experimental Setup

A 0.2 μm layer of $In_{0.53}Ga_{0.47}As$ doped with a silicon concentration of $2x10^{18}$ cm^{-3} was grown by molecular beam epitaxy (MBE) on 500 μm thick commercial grade InP substrates. A 50 nm thick As_2 cap was deposited on MBE grown samples in order to protect the surface from degradation, and samples were shipped and stored under vacuum. The samples were loaded in an Omicron UHV VT-STM chamber with base pressure less than $1x10^{-10}$ Torr, degassed at 180°C for two hours, decapped at 330-360 °C for 2-4 hours, and annealed to 380 °C in order to achieve the pure InGaAs(001)-2x4 surface reconstruction. The (2x4) surface reconstruction was confirmed through low energy electron diffraction (LEED) measurements. STM was used to compare the surface defect density and step densities of decapped samples with atomic hydrogen cleaned samples.

The air exposed samples were dosed with atomic hydrogen at 280°C in UHV to clean and remove the native oxide by using an Oxford Applied Research TC-50 thermal gas cracker. The hydrogen dosing pressure is $1x10^{-6}$ tor; the percentage of atomic hydrogen reaching the sample surface is estimated as 50%, but the exact fraction is unknown because the pressure during dosing includes both H_2 gas and atomic hydrogen. The background H_2 gas should not react with the sample surface, and the atomic hydrogen is believed to remove the surface oxides by reacting with the surface and inducing desorption of oxide species (4). The thermal cracker employs a hot iridium tube to split the H_2 molecules, eliminating contamination that can occur with the heating of tungsten filaments and avoiding the formation of ions typical of plasma sources. Following the cleaning procedure, the samples were transferred in-situ to the STM chamber for atomic scale imaging with an Omicron variable temperature atomic force/scanning tunneling microscopy (AFM/STM) with a base pressure of $2x10^{-11}$ torr. Subsequent annealing of atomic hydrogen cleaned samples at 290 °C for 30 min at $1x10^{-6}$ torr was performed, and the samples were reimaged with STM.

All STM measurements were taken with a sharply etched tungsten tip at room temperature in constant current mode with a tunneling current of 100 pA and an applied sample bias voltage of -3 V in relation to the tip.

Results and Discussion

Part 1: Density Function Modeling of Missing Dimer Defect Sites

The β2(2x4) and α2(2x4) and $In_{0.53}Ga_{0.47}As$(001) reconstructions are models of the ideal and defect unit cells and are shown in Fig. 1 (5). Fig. 1(a) shows the ideal β2(2x4) unit cell containing two adjacent arsenic dimers on the row and one As dimer in the trough. In STM imaging, the row dimers are most readily observed so this unit cell appears as a wide row site in STM (5). Fig. 1(b) shows the α2(2x4) unit cell containing a top row of

single As dimers atoms bonded to tricoordinated In/Ga atoms. This is the most common defect site on the InGaAs(001)-2x4 surface and is often denoted as a missing As dimer site; in STM imaging, this unit cell will appear as a narrow row site (5). The α2(2x4) contains two degenerate isomers, with the arsenic dimers lying to the left or right of the defect missing dimer site. The variation in arsenic dimer locations along the row give rise to the characteristic α2(2x4) zig-zag appearance seen in STM images (5).

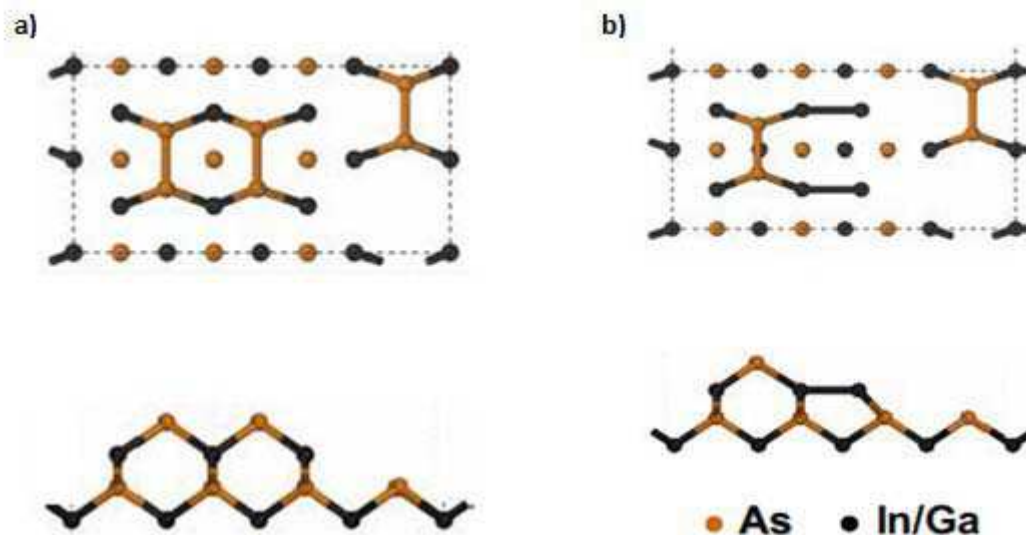Figure 1. DFT calculated models of In$_{0.53}$Ga$_{0.47}$As(001)-(2x4) surface reconstructions. (a) top and side view of β2(2x4) model with a double As dimer on the row. (b) top and side view of the α2(2x4) model with a single As dimer on the row.

In order to determine the effect of the missing dimers on the electronic structure of clean and TMA passivated As-rich InGaAs(001)-(2×4), DFT was employed. All DFT simulations were performed with the Vienna Ab-Initio Simulation Package (VASP) (6,7) using projector augmented-wave (PAW) pseudopotentials (PP) (8,9) and the PBE (Perdew-Burke-Ernzerhof) exchange-correlation functional (10,11). The choice of PBE functional and PAW PP was validated by parametrization runs demonstrating good reproducibility of experimental lattice constants, and bulk moduli for bulk crystalline InGaAs, InAs, and GaAs.

Fig. 2(a) shows an β2(2x4) unit cell containing two row As-dimers while Fig. 2(b) shows an α2(2x4) unit cell with a single row of As-dimers. The structures have been relaxed. The missing dimer defect site in Fig. 2(b) contains a metal-metal dimer bond. TMA can dissociatively chemisorb as either dimethyl aluminum (DMA) or monomethyl aluminum (MMA); the results shown here are for dimethyl aluminum. The DMA DFT full coverage on the (2x4) unit cell contains six total DMA for the double row dimer sites and two DMA for the single dimer row site, since the Al atoms bridge bond between all the As atoms (2).

The calculated density of states (DOS) for the clean surfaces and full coverage DMA are shown in Fig. 2(d) and Fig. 2(e) for the ideal β2(2x4) unit cell and the defect α2(2x4) unit cell. For the ideal unit cell the clean surface has a small conduction band edge state at 0.5 eV. The full coverage DMA/InGaAs(001)-2×4 has a wider bandgap (0.7 eV vs 0.5eV) than the clean surface consistent with passivating the conduction band edge states

on the undercoordinated As atoms. The $\alpha2(2x4)$ unit cell has a substantial conduction band edge state at 0.4 eV, which is not fully passivated by DMA. The results are consistent with $\alpha2(2x4)$ unit cells being problematic for full passivation of the surface by TMA, and the presence of higher D_{it}.
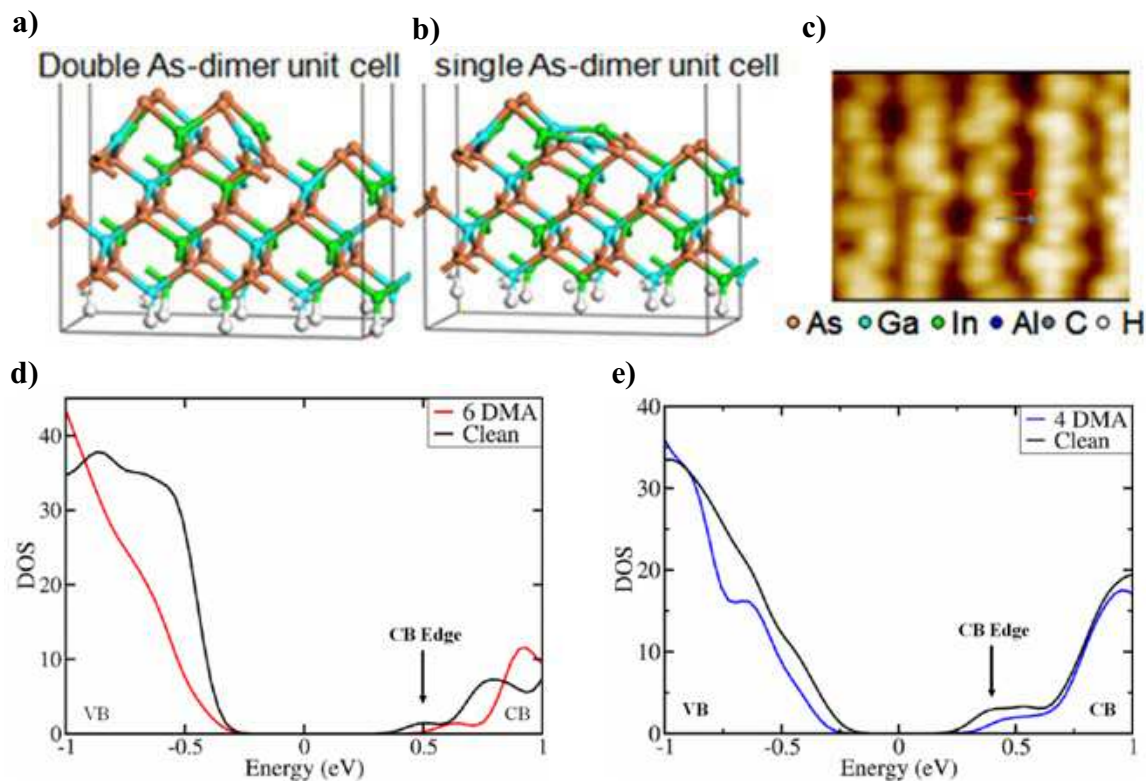

Figure 2. DFT models of Unit Cells on $In_{0.5}Ga_{0.5}As(001)$-2x4. (a) Calculated DFT model of $\beta2(2x4)$ unit cell. (b) Calculated DFT model of $\alpha2(2x4)$ unit cell. (c) Small area STM image prepared at UCSD of $In_{0.53}Ga_{0.47}As(001)$-(2x4) surface. Black arrow points to an occasional wide $\beta2$ (2x4) unit cell and red arrow points to a more frequent majority $\alpha2(2x4)$ single dimer unit cell. (d) Calculated density of states (DOS) plot for $\beta2(2x4)$ unit cell. Complete passivation of band edge states is achieved with 6 dimethyl aluminum (DMA) bonded to the 6 As surface atoms. (e) Calculated density of states (DOS) plot for $\alpha2(2x4)$ unit cell. Conduction band edge states are still seen after all 4 surface As dimers are bonded to DMA.

Part 2: Defects on Decapped $In_{0.53}Ga_{0.47}As(001)$-(2x4)

The filled state STM image of the degassed, decapped, clean $In_{0.53}Ga_{0.47}As(001)$-(2x4) surface reconstruction can be seen in Fig. 3(a). On the $In_{0.53}Ga_{0.47}As$ surface, Fig. 3(a), both $\alpha2(2x4)$ and $\beta2(2x4)$ regions are present as well as many incomplete atomic terraces shown in Fig. 3(b). Regions of $\beta2(2x4)$ and $\alpha2(2x4)$ unit cells can be seen in the Fig. 3(c) and Fig. 3(d) insets taken from the STM image in Fig. 3(a), indicating the annealing procedure yields a mixture of (2x4) surface reconstructions. Note even within $\beta2(2x4)$ regions there are some $\alpha2(2x4)$ unit cells and visa versa.
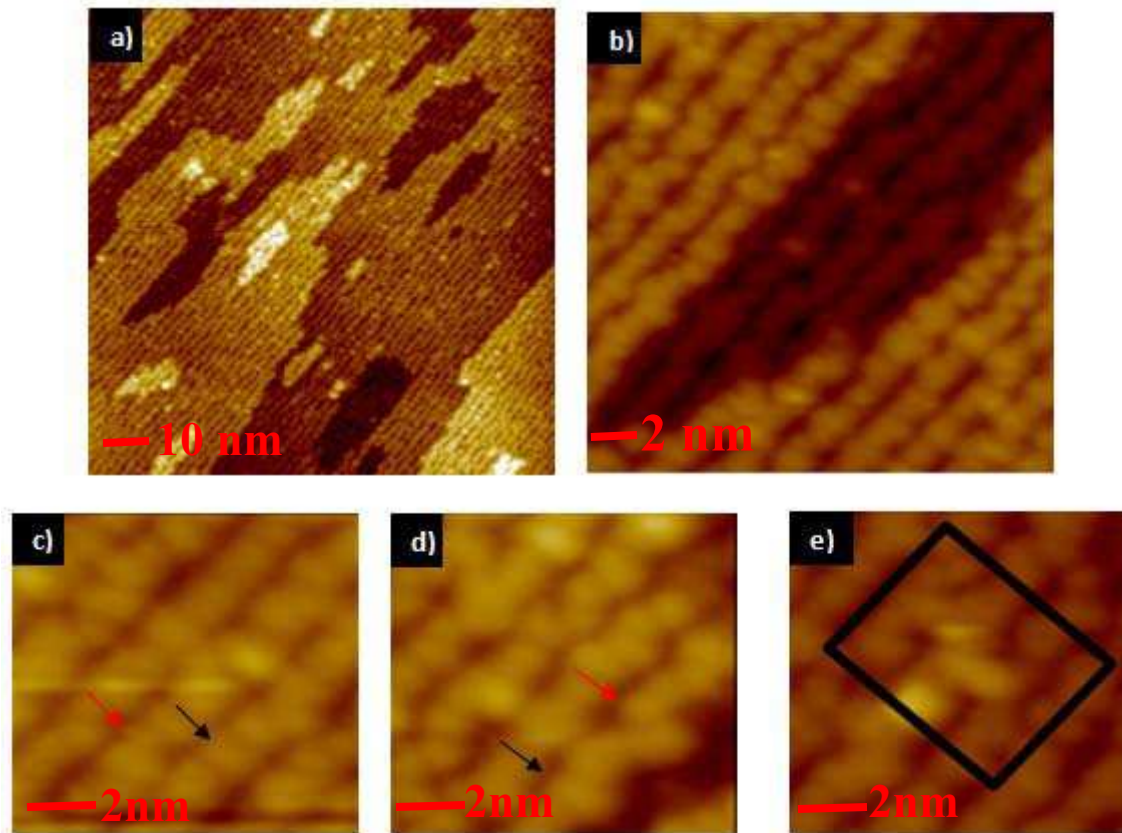
Figure 3. Filled state STM images of decapped $In_{0.53}Ga_{0.47}As(001)$-(2x4). (a) Large area (100 nm x 100 nm) STM image of decapped $In_{0.53}Ga_{0.47}As(001)$-(2x4). (b) Small area (20 nm x 20 nm) of incomplete atomic terraces. (c) Small area (10 nm x 10 nm) of β2(2x4) atomic rows. Black arrow points to a wide unit cell and red arrow points to one of the occasional narrow unit cells. (d) Small area (10 nm x 10 nm) of α2(2x4) atomic rows. Black arrow points to one of the occasional wide unit cells and red arrow points to one of the frequent narrow unit cells. (e) Small area (10 nm x 10 nm) with an adatom trough defect outlined by the square.

An area of 100 nm x 100 nm was manually examined and the structure of 872 unit cells was determined. The total number of α2(2x4) unit cells were counted from all α2(2x4) and β2(2x4) regions, and the result is reported as the average percentage of missing dimer unit cells. From manual examination of the decapped surface, it was determined that $In_{0.53}Ga_{0.47}As(001)$-(2x4) contains an average of 71% single As dimer row α2 unit cells. By dividing the 872 total number of manually counted unit cells into four subgroups, the standard deviation for the examined image was calculated from the subgroup percentages of missing dimers unit cells, and shown in the table. Many incomplete atomic terraces are found on this alloyed surface (1,700/μm^2), increasing surface roughness which may limit charge mobility in MOSFET devices. The lattice mismatch strain caused by In surface segregation may lead to increased missing dimer unit cells (12-18). Alternatively, the In-As bonds are weaker than Ga-As bonds which also might contribute to formation of missing dimer sites. By examining defect densities of surfaces with varying In content and lattice mismatch to the substrates, the two hypothesis can be compared.

Part 3: Defects as a Function of Alloy Concentration

To compare the $In_{0.53}Ga_{0.47}As(001)$-(2x4) surface defect densities to surfaces of similar composition, published images were examined and unit cell structures were manually determined. For each published image, the total number of α2(2x4) unit cells were counted from all α2(2x4) and β2(2x4) regions, and the result is reported as the average percentage of missing dimer unit cells. Table 1 contains the quantified results of α2(2x4) missing dimer unit cells for each STM image in the referenced publications as well as the images from the present study. By dividing the total number of manually counted unit cells into four subgroups, the standard deviation for each examined image was calculated from the subgroup percentages of missing dimers unit cells, and shown in the table. Regions of α2(2x4) unit cells give the characteristic zig-zag pattern seen in the STM images, as shown in Fig. 2(d). The table does not include the relative amounts of α2(2x4) and β2(2x4) regions since that would require examination of extremely large images from multiple locations on the sample and such data is not available. However, it is assumed there will be a correlation between a high number of β2(2x4) unit cells and a high fraction of the surface being purely β2(2x4). After visual examination of the (2x4) surfaces, it is concluded that InAs(001) and GaAs(001) surfaces show the least amount of missing dimer unit cells.

Table 1 also contains quantified results of manually counted adatom trough defects and incomplete atomic terraces found in each STM image. Fig. 3(e) shows the singular adatom trough defect found on the clean decapped $In_{0.53}Ga_{0.47}As(001)$-(2x4) surface. The decapped $In_{0.53}Ga_{0.47}As(001)$-(2x4) surface does not contain a measurable adatom trough defect density, as adatom trough defects are mostly observed for samples prepared in-situ with a high background As_2 pressure. The decapped $In_{0.53}Ga_{0.47}As(001)$-(2x4) surface was prepared without the presence of background As_2 pressure. As explained below, densities of incomplete atomic terraces and adatom trough defects have no correlation to missing dimer unit cells on the examined InAs, GaAs, and InGaAs(001)-(2x4) surfaces, but are noted for reason of increasing surface roughness and inhibiting charge mobility.

GaAs was found to have the lowest amount of defect missing dimer unit cells, with an average of 6%. The average of 6% missing dimer unit cells was calculated from counting total number of α2(2x4) unit cells from all α2(2x4) and β2(2x4) regions found on the GaAs(001)-(2x4) surface. The low amount of missing dimer unit cells is consistent with the published images of GaAs containing large areas of highly ordered β2 (19). Density functional theory (DFT) calculations show the α2 reconstruction is stable for GaAs(001)-(2x4), although this reconstruction has not been reported (5). There are 32,400 adatom defects/μm^2 found in trough regions. No presence of incomplete atomic terraces is seen on the surface possibly due to the small STM image area size (50 x 50 nm).

TABLE I. Defects as a Function of Alloy Concentration.

Alloy Composition	Total Unit Cells	Missing Arsenic Dimer Unit Cells	% Missing Arsenic Dimer Unit Cells	Adatom Trough Defects ($/\mu m^2$)	Density of Incomplete Atomic Terraces ($/\mu m^2$)
Decapped $In_{0.53}Ga_{0.47}As$	872	619	71% +/- 6%	NA	1700
GaAs	1402	90	6% +/- 2%	32,400	NA
$In_{0.27}Ga_{0.73}As$	241	101	42% +/- 18%	10,000	5000
$In_{0.81}Ga_{0.19}As$	993	450	45% +/- 13%	8,800	1200
$In_{0.96}Ga_{0.04}As$	369	238	64% +/- 6%	156,666	NA
InAs	586	146	25% +/- 4%	35,555	NA

Percentage of missing arsenic dimer unit cells, expressed as average +/- one standard deviation, density of adatom trough defects, and density of incomplete atomic terraces found from published and obtained STM images. The average missing dimer unit cells for each image was calculated by counting the total number of α2(2x4) unit cells from an α2(2x4) and β2(2x4) regions. By dividing the total number of manually counted unit cells into four subgroups, the standard deviation for each examined image was calculated from the subgroup percentages of missing dimers unit cells.

$In_{0.27}Ga_{0.73}As(001)$-(2x4) contains an average of 42% missing dimer unit cells, consistent with published images of $In_{0.27}Ga_{0.73}As$ containing large regions of both α2 and β2 surface reconstructions (20). Considering the large missing dimer unit cell standard deviation of 18%, the percentage of missing dimer unit cells on the $In_{0.27}Ga_{0.73}As$ surface may be similar to that found on $In_{0.53}Ga_{0.47}As$ (71% +/- 6%) consistent with the hypothesis of surface strain in the In/Ga alloys leading to the presence of missing dimer unit cells. The surface contains 10,000 adatom defects$/\mu m^2$ in the trough regions as well as 5,000 incomplete atomic terraces$/\mu m^2$, leading to surface roughness.

The $In_{0.81}Ga_{0.19}As(001)$-(2x4) samples contained an average of 45% missing dimer unit cells consistent with $In_{0.81}Ga_{0.19}As$ having regions of both α2 and β2 surface constructions (21). The high standard deviation of missing dimer unit cells, 13%, makes this alloy missing dimer unit cell percentage comparable to both $In_{0.27}Ga_{0.73}As$ (42% +/- 13%) and $In_{0.53}Ga_{0.47}As$ (71% +/- 6%), consistent with the hypothesis of surface strain in the In/Ga alloys leading to the presence of missing dimer unit cells. This In/Ga alloy composition contains the lowest density of trough adatoms (8,800$/\mu m^2$). The images contain atomic steps on the surface, but $In_{0.81}Ga_{0.19}As$ images contain a lower density number of incomplete atomic terraces (1,200$/\mu m^2$) compared to images of $In_{0.53}Ga_{0.47}As$ consistent with there being no correlation between incomplete terrace density and missing dimer unit cells density.

Published images of $In_{0.96}Ga_{0.04}As(001)$-(2x4) contain an average of 64% missing dimer unit cells (22). With the missing dimer unit cell standard deviation of 6%, this alloy concentration surface contains a comparable range of missing dimer unit cells to $In_{0.27}Ga_{0.73}As$ (42% +/- 13%), $In_{0.53}Ga_{0.47}As$ (71% +/- 6%), and $In_{0.81}Ga_{0.19}As$ (45% +/- 13%). There is no trend seen with varying In/Ga alloy composition, as all alloyed surfaces contain large amounts of missing dimer unit cells. This In/Ga alloy composition contains the largest amount of adatom trough defects (157,000/μm^2) with no presence of incomplete atomic steps. The small STM image area size (30 x 30 nm) may lie below the limit of detecting atomic steps on the $In_{0.96}Ga_{0.04}As(001)$-(2x4) surface. The examined STM image of $In_{0.96}Ga_{0.04}As(001)$-(2x4) was taken after quenching the MBE sample at 500° C under high As_2 flux conditions (22). This sample preparation and quenching procedure could lead to the order of magnitude larger adatom trough defects found on the surface consistent with there being no correlation between adatom trough density nor step density with missing dimer unit cells density.

Published images of InAs contain an average of 25% missing arsenic dimer unit cells, with a missing dimer unit cell standard deviation of 4% (23). The average of 25% missing dimer unit cells was calculated from counting total number of α2(2x4) unit cells from all α2(2x4) and β2(2x4) regions found on the InAs(001)-(2x4) surface. These results are consistent with published images of InAs(001)-(2x4) containing a majority of β2 unit cells with a low density of zig-zag α2 regions. The density of InA(001)-(2x4) missing arsenic dimer unit cells is almost 50% lower than on $In_{0.53}Ga_{0.47}As(001)$-(2x4) consistent with the In-As bond being weaker than the Ga-As not being the primary cause of formation of missing dimer unit cells, and strain playing a role in missing dimer unit cell defect formation. However, InAs has a missing dimer concentration is 4x higher than GaAs despite both InAs and GaAs being lattice matched to their substrates and not having surface alloy segregation. The results are consistent with the weaker In-As bond playing a partial role in missing As dimer defect formation. The published images do not contain atomic steps, but adatom defects (35,555/μm^2) arranged in the trough regions between atomic rows are observed and similar in density to GaAs (32,000/μm^2). The small STM image area size (30 x 30 nm) may lie below the limit of detecting atomic steps on the InAs(001)-(2x4) surface. The predominant surface defects present on pure InAs(001) and GaAs(001)-(2x4) surfaces are adatom trough defects, indicating strain from surface segregation in In/Ga alloys does not lead to adatom trough defect formation but instead leads to missing dimer defect unit cell formation.

Part 4: Defects as a Function of Sample Preparation Technique

The use of dry cleaning methods have been found to remove surface contamination and native oxide from III/V surfaces, leaving uniform and highly ordered semiconductor surfaces (24). An atomic hydrogen cleaning method has been found to restore air exposed $In_{0.53}Ga_{0.47}As(001)$-(2x4) surfaces to the order and cleanliness of MBE grown samples. The effects of hydrogen cleaning surface preparation on $In_{0.53}Ga_{0.47}As$ missing dimer defect densities are presented and compared to the sample decapping technique in order to determine which defects are inherently due to strain and which are just due to sample preparation.

Results of atomic hydrogen cleaning on $In_{0.53}Ga_{0.47}As(001)$-(2x4) surface are seen in Fig. 4 and quantifications of defects are found in Table II. Fig. 4(a) shows the hydrogen

cleaned InGaAs surface, which contains large amounts of incomplete terraces in comparison with the InGaAs decapped surface, shown in Fig. 3(a). Atomic hydrogen exposure induced the formation of surface etch pit features. Fig. 4(b) shows the results of hydrogen cleaning with a subsequent annealing process which results in a decrease of etch pit feature density and incomplete atomic terraces, as compared to Fig. 4(a). Etch pit features can be seen in Fig. 4(c) inset taken from STM image shown in Fig. 4(a). Regions of α2 and β2 constructions are present on the hydrogen cleaned surface before subsequent annealing, and shown in Fig. 4(d) inset of Fig. 4(a). The regions of α2 and β2 constructions after the subsequent annealing process are shown in Fig. 4(e) inset of Fig. 4(b). Adatom trough defect sites are not present on surfaces of hydrogen cleaned samples or hydrogen cleaned with subsequent anneal samples, consistent with adatom trough defects mostly observed for samples prepared in-situ with a high background As_2 pressure. Etch pit feature quantification for all sample preparation methods is found in Table III. The decapped $In_{0.53}Ga_{0.47}As(001)$-(2x4) surface does not contain etch pit features but does contain 1700 incomplete atomic terraces/μm^2, leading to surface roughness.
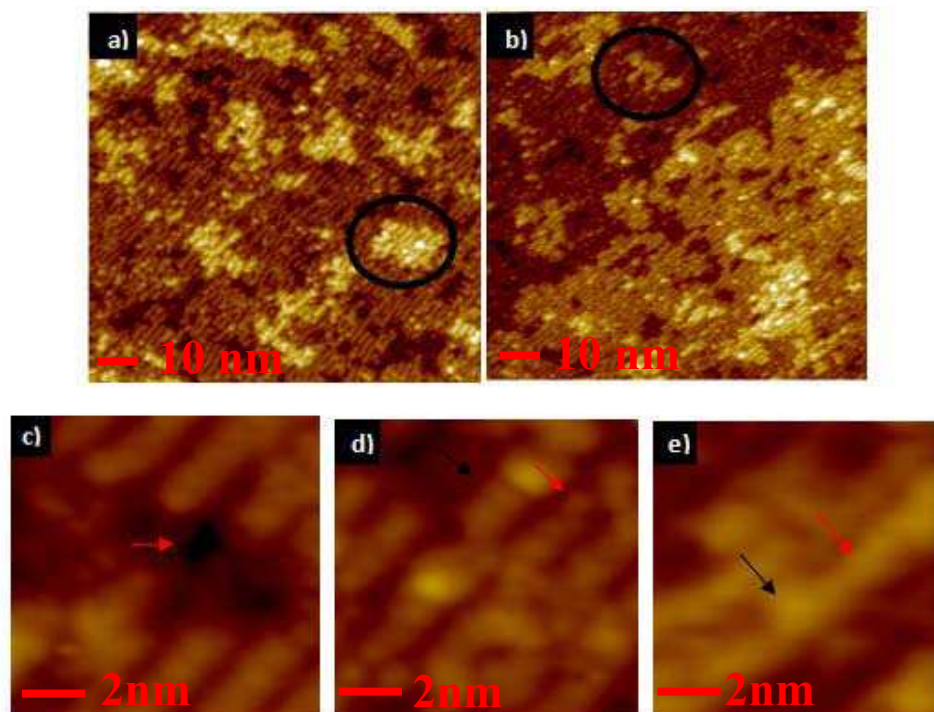

Figure 4. Filled state STM images of atomic hydrogen cleaned $In_{0.53}Ga_{0.47}As(001)$-(2x4). (a) 100 x 100 nm^2 $In_{0.53}Ga_{0.47}As(001)$-(2x4) surface after 30 min 1800 L atomic hydrogen dose at 285° C. Black oval outlines an incomplete atomic terrace. (b) 100 x 100 nm^2 $In_{0.53}Ga_{0.47}As(001)$-(2x4) surface after atomic hydrogen dose and subsequent anneal at 290° C for 30 minutes. Black oval outlines an incomplete atomic terrace. (c) Small area (10 nm x 10 nm) STM image with an etch pit feature indicated by the red arrow. (d) Small area (10 nm x 10 nm) STM image of α2(2x4) and β2(2x4) atomic rows on hydrogen cleaned surface. Black arrow points to a wide unit cell and red arrow points to one of the narrow unit cells. (e) Small area (10 nm x 10 nm) STM image of α2(2x4) and β2(2x4) atomic rows on hydrogen cleaned with post annealed surface. Black arrow points to a wide unit cells and red arrow points to one of the narrow unit cells.

Table II. Missing Dimer Unit Cells as a Function of Sample Preparation Technique.

Prep Method	Unit Cells	Missing Dimer unit cells	% Missing dimer unit cells
Decapping	872	619	71% +/- 6%
Hydrogen Cleaning	806	645	80% +/- 4%
Hydrogen Cleaning with post anneal at 290° C	806	632	78% +/- 5%

Comparison of missing dimer percentages as a function of sample preparation method. Percentage of missing dimer unit cells expressed as average +/- one standard deviation. The average missing dimer unit cells for each image was calculated by counting the total number of $\alpha2(2x4)$ unit cells from all $\alpha2(2x4)$ and $\beta2(2x4)$ regions. By dividing the total number of manually counted unit cells into four subgroups, the standard deviation for each examined image was calculated from the subgroup percentages of missing dimers unit cells.

Table III. Surface Defects as a Function of Sample Preparation Technique

Prep Method	Density of etch pits ($/\mu m^2$)	Density of incomplete terraces ($/\mu m^2$)
Decapping	0	1700
Hydrogen Cleaning	12400	6000
Hydrogen Cleaning with post anneal at 290° C	5600	4500

Comparison of density of etch pits and incomplete atomic terraces as a function of sample preparation method.

As compared to the decapped surface containing 71% missing dimer unit cells, the hydrogen cleaned surface contains 80% missing dimer unit cells. The standard deviations of missing dimer unit cells on the decapped (6%) and hydrogen cleaned (4%) surfaces are sufficiently large that the missing dimer unit cell densities are nearly equivalent. The hydrogen cleaned surface contains 3.5x more incomplete atomic terraces (6000 $/\mu m^2$) compared to the decapped samples as a result of etching. When using atomic H, reduction of the surface oxide results in the clean surface formation of etch pits consistent with desorption of reaction products; selective desorption of As compared to group III atoms is consistent with formation of missing As dimer sites. The hydrogen cleaning procedure with no post annealing leads to the largest density of etch pits, with 12,400 etch pits/μm^2.

The H cleaned and annealed $In_{0.53}Ga_{0.47}As(001)-(2x4)$ surface contains 78% missing dimer unit cells while the hydrogen cleaned surface without annealing contains 80%, indicating missing dimer unit cells does not change by the subsequent annealing process. Post annealing process reduces the number of incomplete atomic terraces (4500/μm^2) by 25% as compared to the H cleaned surfaces and reduced the density of etch pits by 55% to 5600 etch pits/μm^2. More extensive annealing probably could induce further reduction in incomplete terraces and etch pits.

Conclusion

Defect densities on $In_{0.53}Ga_{0.47}As(001)$-(2x4) prepared by several techniques were compared to defect densities from published images of related surfaces of varying In concentration. InAs(001) and GaAs(001) contains the lowest density of $\alpha2(2x4)$ missing dimer unit cells consistent with surface segregation of In during annealing causing stain and leading to increased missing dimer unit cell formation. The missing As dimer defect density is completely uncorrelated with adatoms defect sites in the trough which are mostly observed for samples prepared in-situ with a high background As2 pressure. The missing As dimer defect density is completely uncorrelated with step density and incompletely terrace density, showing the missing As dimer defect density is not related to surface roughness. For $In_{0.53}Ga_{0.47}As(001)$-(2x4), hydrogen cleaning post annealing process significantly reduces the etch pits and incomplete terraces formed from the hydrogen cleaning procedure, although the percentage of missing arsenic dimer unit cells remains high.

DFT modeling has shown that the defect missing dimer sites give rise to conduction band edge states. To effectively passivate these sites it may be possible to convert them to the ideal double dimer unit cells by dosing the sample with a volatile As molecule such as tertiarybutylarsine. Lowering the amount of missing dimer unit cells would potentially decrease the D_{it} in InGaAs based MOSFETs due to the lack of undercoordinated In/Ga atoms, effectively suppressing the conduction band states seen in the DFT models.

References

1. J.A. Del Alamo, *Nature*, **479**, 317 (2011)
2. W. Melitz, T. Kent, A. Kummel, R. Droopad, M. Holland, and I. Thayne, *J. Chem. Phys.*, **136**, 154706 (2012)
3. Y. Hwang, R. Engel-Herbert, and S. Stemmer, *ApPhL*, **98**, 052911 (2011)
4. W. Melitz, J. Shen, T. Kent, and A. Kummel, *JAP*, **110**, 013713 (2011)
5. J. Shen, D. Winn, W. Melitz, J. Clemens, and A. Kummel, *ECS Trans.*, **16**, 463 (2008)
6. G. Kresse, and J. Furthmuller, *Comput. Mater. Sci.*, **6**, 15-50 (1996)
7. G. Kresse, and J. Furthmuller, *Phys. Rev. B*, **54**, 11169-11186 (1996)
8. J.P. Perdew, K. Burke, and M. Ernzerhof, *Phys. Rev. Lett.*, **77**, 3865-3868 (1996)
9. J.P. Perdew, K. Burke, and M. Ernzerhof, *Phys. Rev. Lett.*, **78**, 1396-1396 (1997)
10. P.E. Blochl, *Phys. Rev. B*, **50**, 17953-17979 (1994)
11. G. Kresse, and D. Joubert, *Phys. Rev. B*, **59**, 1758-1775 (1999)
12. J. Mirecki Millunchick, A. Riposan, B.J. Dall, C. Pearson, and B.G. Orr, *SurSc*, **550**, 1-7 (2004)
13. G. Grenet, E. Bergignat, M. Gendry, M. Lapeyrade, and G. Hollinger, *SurSc*, **352-354**, 734-739 (1996)
14. M. Mesrine, J. Massies, C. Deparis, N. Grandjean, E. Vanelle, and M. Leroux, *J. Cryst. Growth*, **175/176**, 1242-1246 (1997)
15. J. Nagle, J.P. Landesman, M. Larive, C. Mottet, and P. Bois, *J. Cryst. Growth*, **127,** 550-554 (1993)
16. S. Yu. Karpov, and Yu. N. Makarov, *Thin Solid Films*, **380**, 71-74 (2000)

17. K. Yamaguchi, T. Okada, F. Hiwatashi, *Appl. Surf. Sci.*, **117/118**, 700-704 (1997)
18. F.S. Aguirre-Tostado, M. Milojevic, C.L. Hinkle, E.M. Vogel, and R.M. Wallace, *ApPhL*, **92**, 171906 (2008)
19. B. Joyce, and D. Vvedensky, *Mater. Sci. Eng., R.*, **46**, 127 (2004)
20. Lee E Sears, "Investigations of Surface Reconstructions and Inverse Stranski Krastanov Growth in InGaAs Films," *Dissertation*,University of Michigan (2009)
21. J. Mirecki Millunchick, A. Riposan, and B. J. Dall, *ApPhL*, **83**, 1361 (2003)
22. P.A. Bone, J.M. Ripalda, G.R. Bell, and T.S. Jones, *SurSc*, **550**, 1 (2006)
23. C. Ratsch, W. Barvosa-Carter, F. Grosse, and J. H. Owen, *Phys. Rev. B,* **62**, R7719 (2000)
24. E. J. Petit and F. Houzay, *J. Vac. Sci. Technol., B*, **12**, 547 (1994)